Hybrid Advances 3 (2023) 100045

Contents lists available at ScienceDirect

Hybrid Advances

journal homepage: www.journals.elsevier.com/hybrid-advances

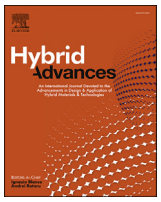

Design of novel hybrid 2D nanomaterials for optical, optoelectronic and micro-electro-mechanical systems applications

V.W. Elloh [a,b,*], E. Okoampa Boadu [b], G. Gebreyesus [c], A.K. Mishra [a], D. Dodoo-Arhin [d], A. Yaya [d]

[a] Department of Physics, University of Petroleum and Energy Studies (UPES), Dehradun, India
[b] Department of Biomedical Engineering, Koforidua Technical University, Koforidua, Ghana
[c] Department of Physics, University of Ghana, Legon, Ghana
[d] Department of Materials Science and Engineering, University of Ghana, Legon, Ghana

ARTICLE INFO

Keywords:
Hybrid
Microelectromechanical
Design
Novel hybrid 2D nanoheterostructures
Optoelectronics

ABSTRACT

Novel hybrid 2D class of ternary nanoheterostructures have been designed by mixing aluminium nitride (AlN), boron nitride (BN) with 2D graphene with the aim of designing innovative 2D nanoheterostructures for applications in electronics and other industries. The structural stability and electronic properties of these nanoheterostructures have been analysed using "first-principles based calculations done in the framework of density functional theory. Different structural patterns have been analysed to identify the most stable nanoheterostructures. It has been found to be more energetically favourable that the aluminium nitride and boron nitride atom chains occupy the positions of the carbon atoms in a clustered pattern in the nanoheterostructures. Carbon atom chains sandwiched between aluminium nitride and boron nitride chains of atoms is a preferred choice over isolated chains of BN, AlN and CC in the nanoheterostructures. The calculated band gaps of the novel nanoheterostructures are found to be 0.87, 0.43 and 0.65 eV respectively. These novel hybrid 2D nanoheterostructures are energetically favoured materials with both direct and indirect band gaps. They have potential applications in nanoscale semiconducting and optoelectronic devices, notably optical, optoelectronic and micro-electro-mechanical systems.

1. Introduction

Boron nitride exhibits a graphite-like hexagonal (h-BN) structure with space group P63/mmc (no. 194) at ambient conditions [1]. Depending on the pressure and temperature conditions, a transformation to the wurtzite [2–4] or cubic sphalerite [5–7] structure type may appear. The cubic variety of boron nitride has high hardness, high melting point, high thermal conductivity, large bulk moduli and it is used in cutting tools, grinding, as abrasive material [8–10], in protective coatings [11] and electronic devices [12].

In recent studies, solid solutions of boron nitride were doped with different elements. The most common dopant is carbon [13–15]. Also, doping with silicon was investigated experimentally and theoretically [16,17]. Recently, doping with P, S, O, F and Cl were investigated using ab initio methods [18]. Mostly, doping is introduced to modify the electronic properties of h-BN. Group III semiconductor nitrides (AlN, InN, GaN) are among the most important materials for electronic and optoelectronic applications [19–22]. Doping with Al was investigated previously [23,24]. To improve the machinability of AlN-based materials, while maintaining their desirable properties, composites with h-BN are prepared [25].

Considering previous studies of B–Al–N solid solution, the most recent was conducted for h-BN and wurtzite type of structure in B–Al–N [26], where the impact of composition on structure and electronic properties was analysed. Zhang et al. [26] investigated B–Al–N thin films both in theory and experiment, while a purely theoretical investigation was conducted for a 6.25% concentration of the Al in the BN [27]. BN nanotubes, nanosheets and monolayers were doped with Al [28–30] and investigated theoretically and experimentally synthesized in the form of thin films [31,32]. Also, the structural and electronic properties of the BxAl1-xN (x = 0.6, 0.25, 0.50 0.75) solid solution were investigated by first-principles calculations, but only for the wurtzite structure type [33,34]. Similarly, only for the cubic phase of AlN (sphalerite structure type) the influence of the addition of boron on the mechanical, electronic and thermodynamical properties was investigated theoretically [35–39]. Furthermore, the sphalerite AlN was co-doped with Y and B and

* Corresponding author. Department of Physics, University of Petroleum and Energy Studies (UPES), Dehradun, India.
E-mail address: vanw.elloh@ktu.edu.gh (V.W. Elloh).

https://doi.org/10.1016/j.hybadv.2023.100045
Received 31 December 2022; Received in revised form 18 April 2023; Accepted 13 May 2023
Available online 15 May 2023

investigated theoretically [40]. Besides wurtzite and sphalerite structure types, the doped Al1-xBxN system was investigated inside of possible diamond-like novel BN allotrope adopting Pmn21 space group [41]. The magnetic and electronic properties of the wurtzite BN doped with Ti, V and Cr atoms were investigated using theoretical methods [42–49].

Modern semiconductor devices have revolutionized wide-ranging technologies such as electronics, lighting, solar energy and communication [50]. The semiconductor industry employs Si to fabricate electronic circuits and GaAs, GaN and other group III–V materials for optoelectronics [51], with typical substrates consisting of wafers manufactured at high temperatures. Recent research has focused on a new generation of atomically thin films of semiconducting materials. Guided by the rise of graphene [52–55] a broad family of two-dimensional (2D) semiconducting materials have been fabricated in monolayer, bilayer and few-layer forms [56,57]. Monolayer and few-layer semiconductors possess novel combinations of optical and electronic properties [55–59] and thus present a unique opportunity in condensed matter physics research and semiconductor devices. A new physics arises in 2D semiconductors, largely due to the peculiar electronic structure and screening effects in 2D systems. As the techniques for growing 2D materials on large areas advances, the new properties of these materials may enable a paradigm shift in semiconductor-based technologies and lead to flexible and ultrathin electronic and optoelectronic devices [59–61]. The 2D semiconductor materials in the form of monolayer, bilayer and few-layers give rise to new electronic and optoelectronic devices with ultrathin thickness and flexibilities due to new physics behind their electronic structures and the screening in the 2D systems [62]. These two-dimensional materials with anisotropy can open new era of optoelectronic technology due to their orientation and frequency dependent properties. The 2D based layered materials are useful in electronic devices, sensors and energy systems [63,64]. 2D monolayers have outstanding chemical stability, high anisotropy and high thermal and dynamic stabilities [65,66].

Dimensionality plays a fundamental and important role in material research. This does not only refer to the structural features of the materials of interest, but also determines many of their properties [67]. The successful isolation of graphene from bulk graphite and discoveries of its exceptional physical properties, including ultrahigh electron mobility, anomalous quantum Hall effect and ballistic charge carrier transport, have initiated intensive interests of various scientific communities to 2D materials [52,53]. 2D materials are infinite crystalline structures made of periodic units in two dimensions (in-plane) but having atomic thickness in the third dimension (out-of-plane).

Several outstanding properties of 2D materials are well known. Among them are unique electronic and optical properties, e.g., from its bulk to a monolayer structure, a 2D material evolves from indirect bandgap to direct bandgap transition and improves the photoluminescence quantum yield up to a factor of about 10^4 due to the absence of interlayer interactions [68], quantum confinement in the direction perpendicular to 2D material planes. This factor promotes electrons, excitons and phonons to have a longer mean free path and governs ballistic in-plane transport without scattering or diffusion [69,70], 2D geometry is well compatible with the present device design and fabrication standards in electronic industries [71] and high mechanical strength and flexibility. Hence, 2D materials should have great potentials for applications in electronic, optoelectronic, sensing, flexible devices and many other fields.

2D materials constructed by light and nonmetal atoms possess diverse structures and property variations and have attracted prime attentions in designing new 2D materials with tailored electronic properties and specific functionalities. Their atom sizes are close enough to each other and can effectively form conjugated structures. This characteristic is considered to be a critical factor in electronic and bandgap properties engineering of 2D materials. Motivated by these interesting consequences, the structural properties, phonon-dispersion, elemental projected electronic band structures and optical properties of the novel 2D structures comprising graphene, nitrides of aluminium and boron are explored using first-principles calculations in this work. This design covers the state of the art in the optical and electronic properties of 2D materials with focus on semiconducting systems.

2. Computational details

We used the PWSCF code of the Quantum ESPRESSO [72] to obtain the results of first-principles calculations based on plane-wave basis sets and Perdew-Burke-Ernzerhof (PBE) Vanderbilt Ultrasoft Pseudopotentials [73]. Brillouin zone sampling was performed within the Monkhorst-Pack scheme [74] using $5 \times 5 \times 1$ Γ-centred grids for geometry relaxations. We adopted a $9 \times 9 \times 1$ k-grid mesh in the Brillouin zone of the supercell (2×2) for the geometry optimization. The non-self-consistent calculations were performed with the converged wave functions and a much denser $(12 \times 12 \times 12)$ k-point mesh was chosen to obtain very smooth band structure calculated in $\Gamma - X - M - N - \Gamma$ direction of the hexagonal Brillouin zone. The supercell is oriented along the z-axis and unit cell geometry with vacuum space of 15°A thickness in both x- and y-directions is allowed to ensure negligible interactions between the sheet and its periodic images. The lattice and atomic positions were fully relaxed until the residual force was less than 0.4×10^{-2} Ry bohr^{-1}($\sim$ 0.1 eV Å^{-1}). The cut-off energy for plane waves was set to 30 Ry. Due to the non-ignorable impact of the vdW-like interaction in the structure, we introduced the Grimme's D3 correction term [75] to correct the dispersion in the computations of the structures. This approach provides reliable outcomes for layered structures.

3. Results and discussions

3.1. Geometry and structural stability

In this section, we discuss the structures, different configurations and structural stability of nanoheterostructures investigated in the current work. We investigated three different configurational patterns of CC:AlN:BN nanoheterostructures. Firstly, we acted by replacing alternate carbon (CC) layers with aluminium nitride (AlN) followed by boron nitride (BN) layers in a 2D graphene sheet comprising 32 atoms, Fig. 1(a). Secondly, we replaced single CC layer with single layer of AlN atoms and leaving two CC layer of atoms intact and then replaced the next CC layer with single BN layer, Fig. 1(b). Similarly, in the third configuration, Fig. 1(c), AlN and BN layer atoms replaced two CC layers in an adjacent pattern.

Observations from Fig. 1 revealed that all the structures remain intact after optimization. We evaluated the stability of the CC:AlN:BN nanoheterostructures by calculating the formation energy of each substitution to find the energetically most favourable configurations, as

$$\Delta E = E_{CC:AlN:BN} - N_C E_C - N_{Al} E_{Al} - N_N E_N - N_B E_B \quad (1)$$

where $E_{CC:AlN:BN}$ is the total ground-state energy of the CC:AlN:BN nanoheterostructure; E_C, E_{Al}, E_N and E_B are the ground-state energies of carbon, aluminium, nitrogen and boron atoms, respectively. N_C, N_{Al}, N_N and N_B are the number of carbon, aluminium, nitrogen and boron atoms in the nanoheterostructure respectively.

The calculated formation energies per atom for each nanoheterostructure is tabulated in Table 1. Observations showed that for all concentrations, the formation energy is lower when carbon atoms or boron and aluminium nitride atoms form clusters in the nanoheterostructure. Therefore, it is energetically more favourable that carbon atoms or boron and aluminium nitride atoms occupy clustering positions in the novel 2D nanoheterostructures. In addition, all of the newly fabricated 2D nanoheterostructures have negative formation energies, which shows that these AlN:CC:BN, AlN:CC:CC:BN and CC:BN:AlN:CC structures are thermodynamically stable. Further, we calculated the formation energy per atom for AlN and BN sheets and had

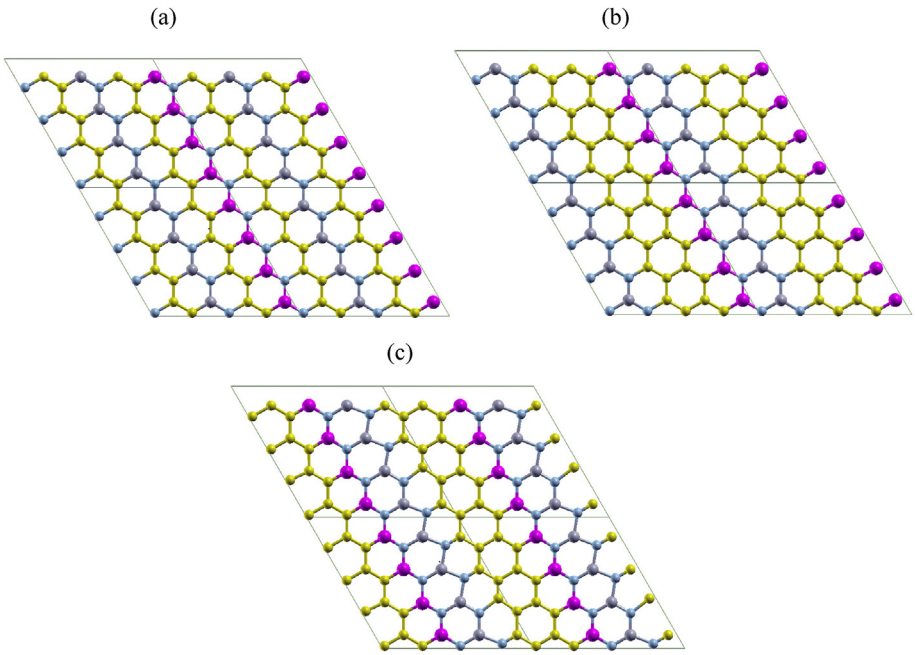

Fig. 1. Simulated nanoheterostructures of CC:AlN:BN. (a) AlN:CC:BN nanoheterostructure configuration; (b) AlN:CC:CC:BN nanoheterostructure configuration; (c) CC:BN:AlN:CC nanoheterostructure configuration. A 2 × 2-unit cell is shown for better representation of chemical bonds and structures, where a 32-atom CC supercell is doped with AlN and BN atoms with carbon concentrations of 50% used in the calculations.

Table 1
Formation energy per atom calculated using Equation (1) for ternary $Al_xN_{y/2} : CC_{1-x-y-z} : B_zN_{y/2}$, $(x + y + z = 0.5)$ compounds.

Nanoheterostructure	% doping of atoms	formation energy/atom (eV)
(a) AlN:CC:BN	0.5	−5.619
(b) AlN:CC:CC:BN	0.5	−5.876
(c) CC:BN:AlN:CC	0.5	−5.948
h-BN		−1.171
AlN		−1.596
CC		0.008

Table 3
Optimized Bond Lengths of the AlN, CC, BN and their Nanoheterostructures.

Nanoheterostructure	Bond lengths (Å)					
	Al–C	Al–N	C–C	B–N	C–N	B–C
AlN		1.786				
CC			1.421			
BN				1.451		
AlN:CC:BN	1.993	1.841	1.395	1.390	1.383	1.481
AlN:CC:CC:BN	1.907	1.743	1.438	1.559	1.463	1.568
CC:BN:AlN:CC	1.981	1.932	1.434	1.593	1.333	1.644

their values to be −1.596 and −1.473 eV respectively. They are far greater than the formation energies per atom in Table 1 for all the novel nanoheterostructures designed, indicating new nanoheterostructures are more stable than them.

The computations indicate that in AlN:CC:CC:BN and CC:BN:AlN:CC nanoheterostructures, clustering of CC chains and AlN and BN chains together is favoured over scattering of CC and AlN and BN chains within the ternary structures. AlN:CC:CC:BN and CC:BN:AlN:CC clustered configurations being more stable compared to isolated chain configuration, AlN:CC:BN. In Table 2, it is observed that as a result of incorporating AlN and BN layers in 2D CC sheet, the CC supercell widens and the volume of the simulated 32-atom AlN:CC:CC:BN, CC:BN:AlN:CC and AlN:CC:BN novel nanoheterostructures increased from initial volume of 582.091 for 2D CC sheet to 802.472, 803.999 and further to 837.708 $Å^3$ respectively.

In the AlN:CC:BN configuration investigated in Table 3, we observed that C–C bond and B–N bond are of slightly smaller lengths, 1.395 and 1.390 Å, respectively as compared to that in the graphene CC and boron nitride sheets, 1.421 and 1.451 Å respectively. This is indicative of stiffer bonding in AlN:CC:BN configuration and preferring isolated chains of CC, BN and AlN over bigger clusters of the same atoms in graphene and boron nitride sheets. However, in AlN:CC:CC:BN, shorter Al–N bond length of 1.743 Å compared with 1.786 Å in AlN sheet and hence stronger bond is found to be indicative of more stability of segregated layered structures of BN and AlN. Moreover, C–C, C–N and B–N bonds are found to be more stiffer in CC:BN:AlN:CC structure than B–N, C–C and Al–N respectively in pristine boron nitride, graphene and aluminium nitride 2D structures respectively, resulting in their stability and rigidity due to strong covalent bonding characteristics. The nanoheterostructures have outstanding chemical stability, high anisotropy and high thermal and dynamic stabilities.

3.2. *Electronic properties*

The electronic band structures at high-symmetry k-points for AlN:CC:BN, AlN:CC:CC:BN and CC:BN:AlN:CC nanoheterostructures are

Table 2
Optimized lattice parameters, cell volume and energy band gap of different nanoheterostructures.

Nanoheterostructure	a(Å)	b(Å)	c(Å)	V($Å^3$)	E(eV)	Space Group	Point Group	Crystal System
CC	9.878	8.556	6.889	582.091	0.00	P6/mmm [191]	6/mmm	Hexa-gonal
AlN:CC:BN	12.570	9.622	6.924	837.708	0.87	$P6_3$/mmc [194]	6/mmm	Hexa-gonal
AlN:CC:CC:BN	13.139	8.748	7.009	802.472	0.43	$P6_3$/mmc [186]	6 mm	Hexa-gonal
CC:BN:AlN:CC	12.228	9.937	6.616	803.999	0.65	$P6_3$/mmc [194]	6/mmm	Hexa-gonal

shown in Fig. 2(a–c). The band gaps of pristine AlN, BN and CC 2D sheets are found to be 3.269, 4.270 and 0.000 eV respectively. The calculated band gaps of AlN:CC:BN, AlN:CC:CC:BN and CC:BN:AlN:CC nanoheterostructures are found to be 0.87, 0.43 and 0.65 eV respectively. Observations show that, Fig. 2(a) has a direct band gap while Fig. 2(b and c) show indirect band gaps at the M-point. These nanoheterostructures are useful for applications in electronic devices such as sensors and energy systems. The novel 2D nanoheterostructures have tunable band gaps and possess potential applications in many fields, notably optical, optoelectronic and micro-electro-mechanical systems. We noted that incorporation of BN and AlN chains into graphene CC 2D layers lowers the electronic band gaps of BN and AlN sheets. On the other hand, it opens gaps in the 2D CC:AlN:BN nanoheterostructures. The gaps occur due to mixed hybridization of valence states of Al, B and N with that of C atoms. The calculated values of the band gaps, E_g, are presented in Table 2.

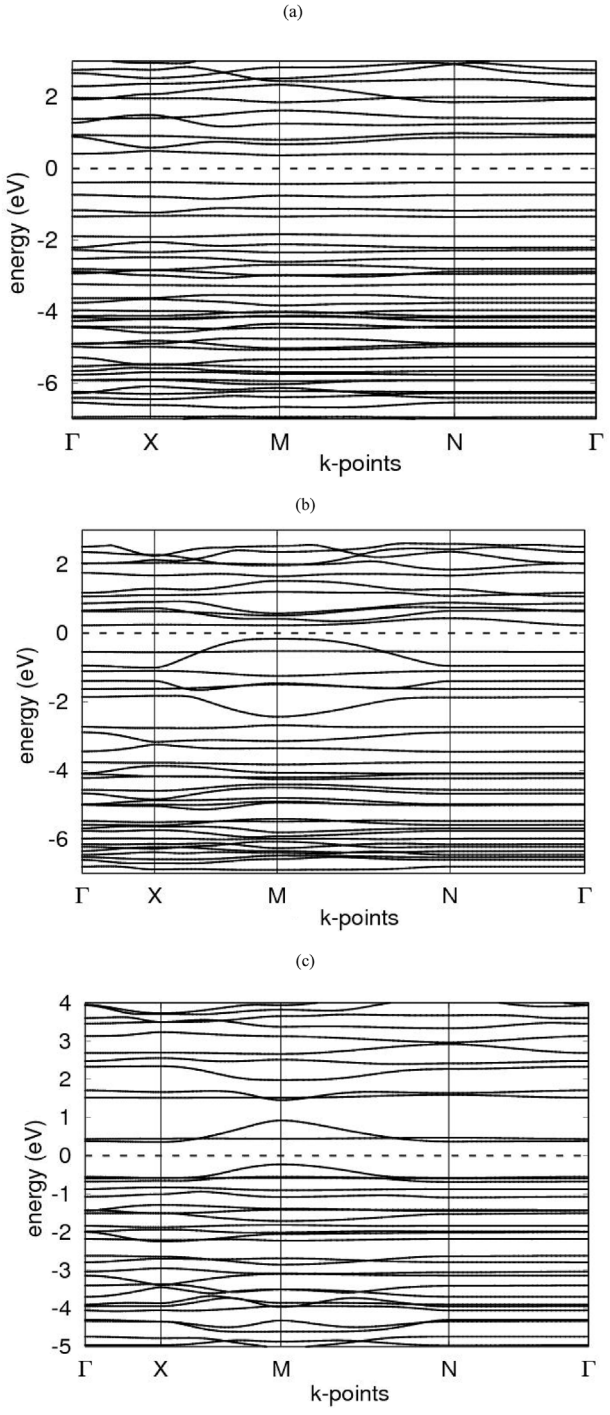

Fig. 2. Calculated band structures at high-symmetry k-points for (a) AlN:CC:BN, (b) AlN:CC:CC:BN and (c) CC:BN:AlN:CC nanoheterostructure configurations.

Detailed analysis of the nature of interactions and origin of gaps in these nanoheterostructures was performed. We plotted the DOS and projected DOS (p-DOS) of AlN:CC:BN, AlN:CC:CC:BN and CC:BN:AlN:CC nanoheterostructures as shown in Fig. 3(a–c) and Fig. 4(a–c) respectively to carry out the analysis. Visualizing the atomic orbitals, we noted that the DOS near the gaps is essentially of pz character occurring from the antibonding and bonding of Al and N states hybridizing with those of pz states of carbon. Similar hybridization of states is observed due to boron atoms in the nanoheterostructures. The position of the energy gap due to such hybridization is very crucial such that upon doping of CC by different coverage or configurations of AlN or BN, the energy gap occurs at the E_F. For the purposes of the present work, the Figures (3 & 4) show only positive contributions to the total and partial spin-polarized states of electrons for the nanoheterostructure configurations. In order to fully understand the role of each of the contributions from the atomic-orbitals to the electron density of states (DOS) of nanoheterostructure configurations, Fig. 5(a, b & c) show in the same plot the DOS and TDOS for the novel hybrid 2D class of ternary nanoheterostructures (see Fig. 6(a–c) are the total electronic density of states (t-DOS) with fermi energy level set at zero for the nanoheterostructures.

For the ternary structures, the calculated band gaps are given in Table 2. From the electronic band structure plots analysis, we observed that these structures are direct band gap materials with band gap values of 0.87, 0.43 and 0.65 eV, with the valance band and conduction band to be located at the γ k-point. A comparison with the band structures of CC graphene, BN and AlN with the new 2D nanoheterostructures shows that new bands are formed due to hybridization of states in the new 2D ternary compounds. These new forms of hybridized 2D materials will facilitate the development of band gap engineering and applications, in particular, in nanoelectronics and nano-optics.

3.3. *Charge density*

The charge density plots in Fig. 7 show a homogenous charge distribution among the nitrogen, boron, aluminium and carbon atoms signifying that a significant chemical interaction took place. In terms of charge distribution, there is a uniform sharing between the nitrogen and carbon atoms with respect to electronegativity values of 3.04 and 2.55. There is also an excellent charge distribution between the aluminium and boron atoms because of similar electronegativity values of 1.61 and 2.04 respectively. The PDOS in Fig. 4 indicate that the p-orbitals of carbon, boron, aluminium and nitrogen atoms all contributed significantly to the total density of states. The reason for this can be traced back to the charge density plots in Fig. 7. The plots show higher density of charges around the carbon and nitrogen atoms. This is apparently due to nitrogen having comparable electronegativity value to that of carbon. As a result, the carbon and nitrogen atoms draw more electrons to themselves.

3.4. *Optical properties calculated ultra violet optical absorption*

Fig. 8(a–c) show the calculated anisotropic optical absorption spectra for (a) AlN:CC:BN, (b) AlN:CC:CC:BN and (c) CC:BN:AlN:CC nanoheterostructure configurations. The nanoheterostructures have absorption for visible and UV frequencies in both parallel and perpendicular field directions. In the optical absorption spectra of the nanoheterostructures, the large anisotropy is observed between parallel and perpendicular field directions. For AlN:CC:BN, the infrared and visible frequencies having photon energies below 5.58 eV and above 7.35 eV, the nanoheterostructure shows negligible optical absorption in both cases, i.e., in-plane direction and out-plane direction to field. This nanoheterostructure material shows the strongest absorption peak at photon energy of 6.80 eV in the ultra-violet region for the out-plane

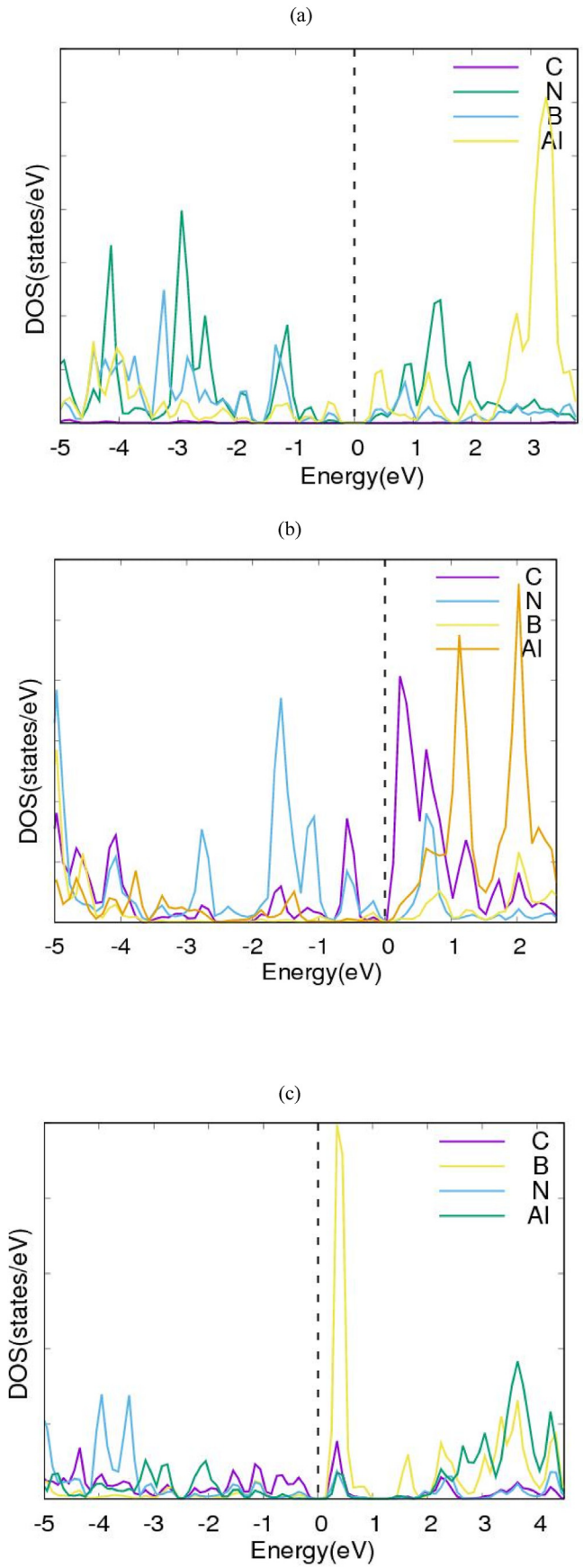

Fig. 3. Electronic density of states (DOS) for (a) AlN:CC:BN, (b) AlN:CC:CC:BN and (c) CC:BN:AlN:CC nanoheterostructure configurations, with fermi energy level set at zero.

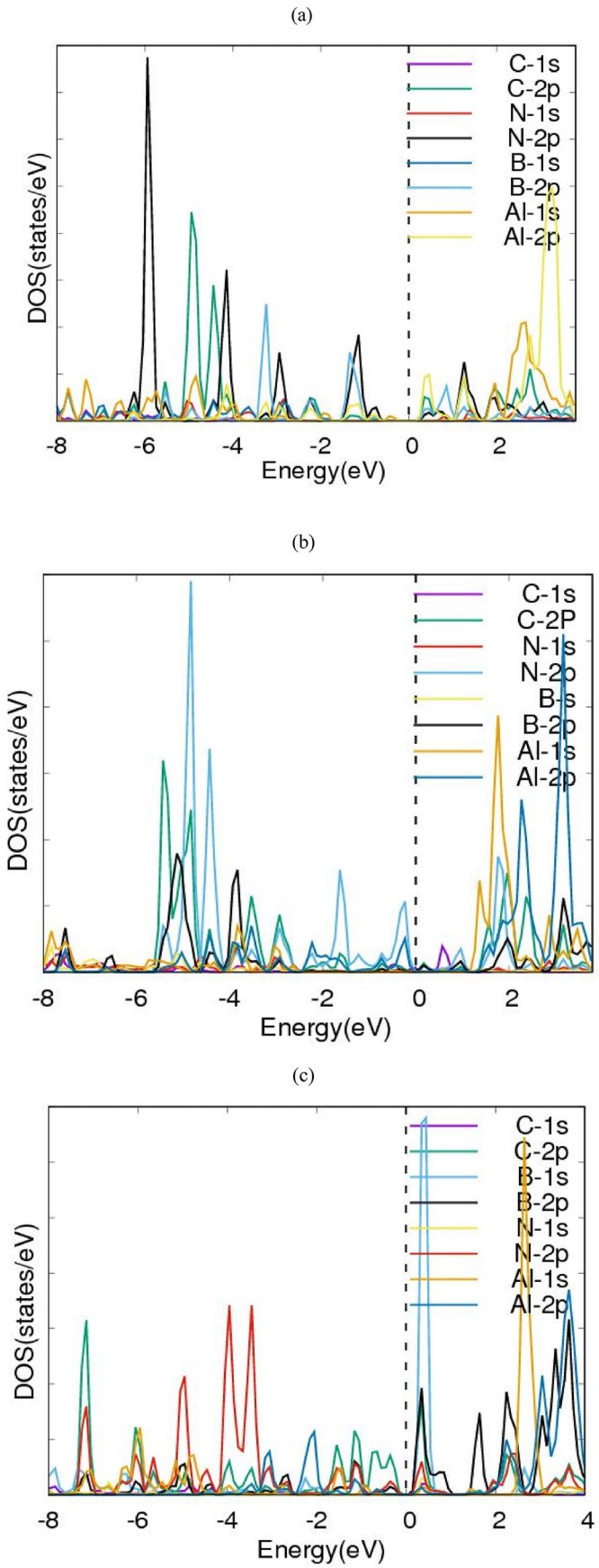

Fig. 4. Projected density of states (p-DOS) for (a) AlN:CC:BN, (b) AlN:CC:CC:BN and (c) CC:BN:AlN:CC nanoheterostructure configurations, with fermi energy level set at zero.

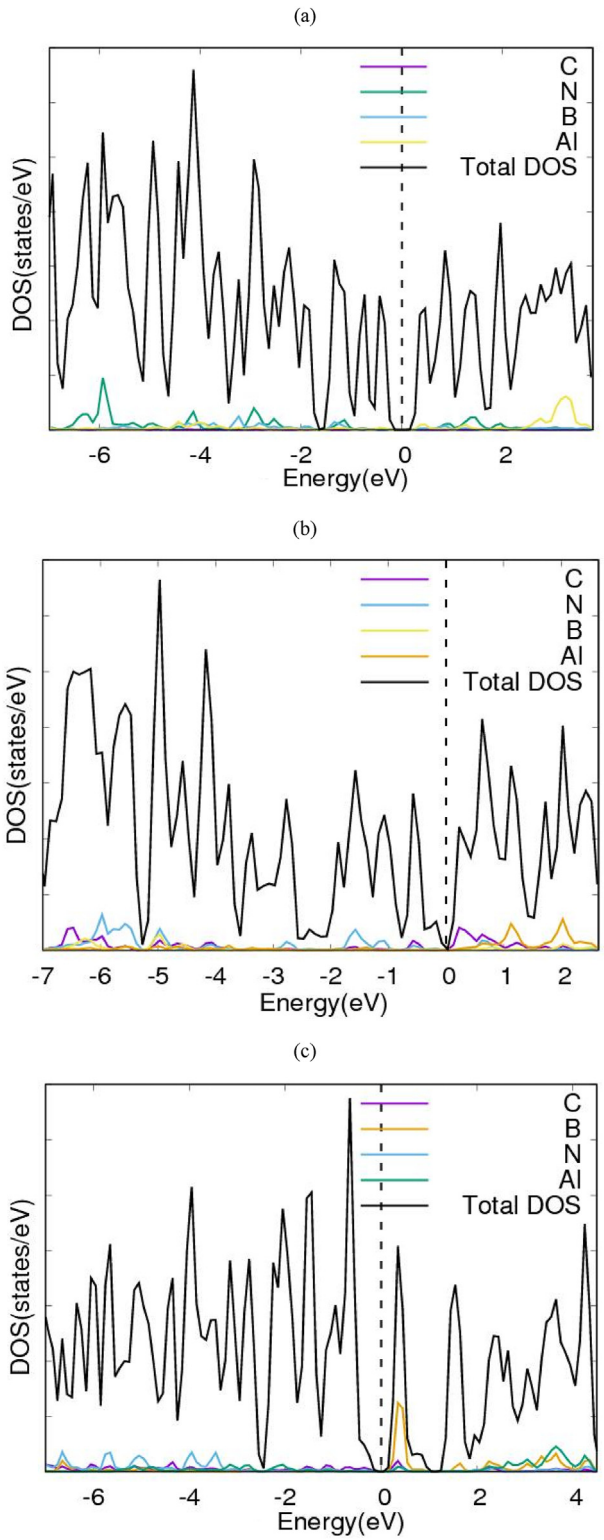

Fig. 5. Projected electronic density of states (DOS) and total DOS (t-DOS) superimposed for (a) AlN:CC:BN, (b) AlN:CC:CC:BN and (c) CC:BN:AlN:CC nanoheterostructure configurations. The Fermi energy level, E_F, is set as zero on the energy scales.

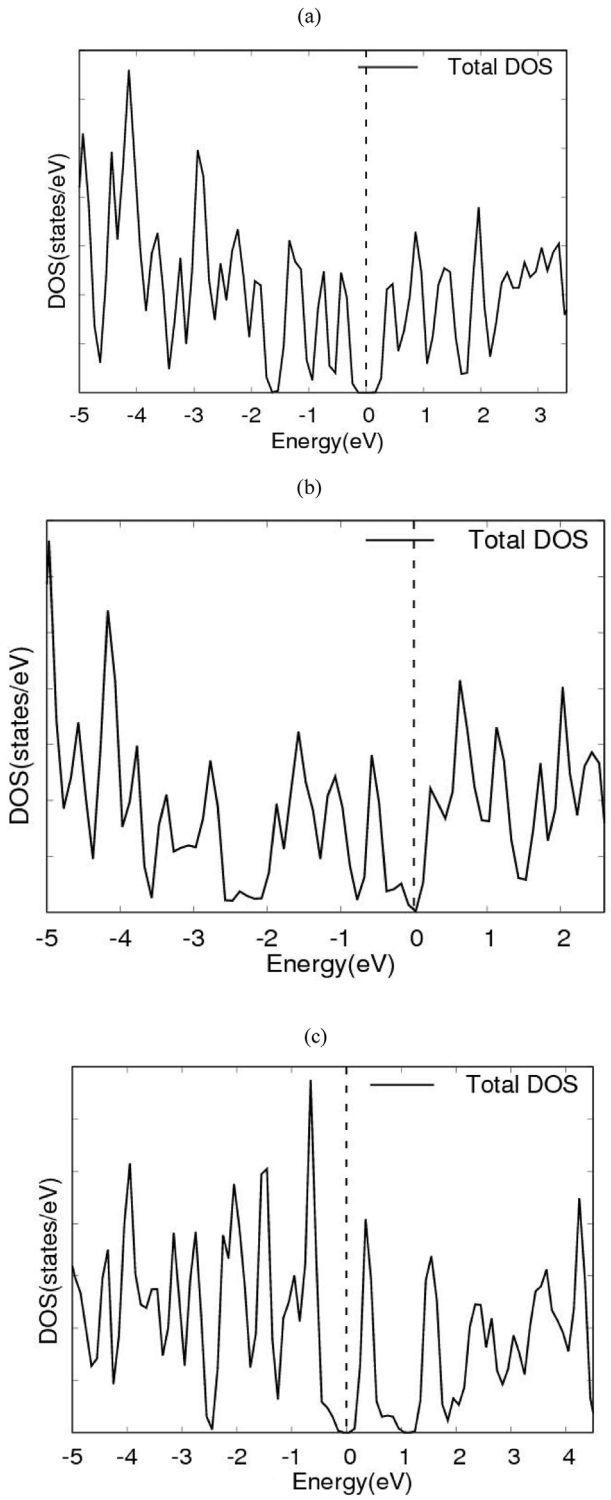

Fig. 6. Total electronic density of states (t-DOS) with fermi energy level set at zero for (a) AlN:CC:BN, (b) AlN:CC:CC:BN and (c) CC:BN:AlN:CC nanoheterostructure configurations.

direction, i.e., perpendicular direction. In the AlN:CC:CC:BN nanoheterostructure, the infrared and visible frequencies having photon energies below 5.71 eV and above 7.08 eV, the nanoheterostructure shows negligible optical absorption in both cases. This nanoheterostructure material shows the strongest absorption peak at photon energy of 6.12 eV in the ultra-violet region for the out-plane direction. Concerning CC:BN:AlN:CC nanoheterostructure, the infrared and visible frequencies having photon energies below 5.85 eV and above 7.21 eV, the nanoheterostructure shows negligible optical absorption in both in-plane and out-plane directions to field. This nanoheterostructure material shows the strongest absorption peak at photon energy of 6.26 eV in the ultra-violet region for the out-plane direction. These 2D nanoheterostructures with high anisotropy and stability can open new era of

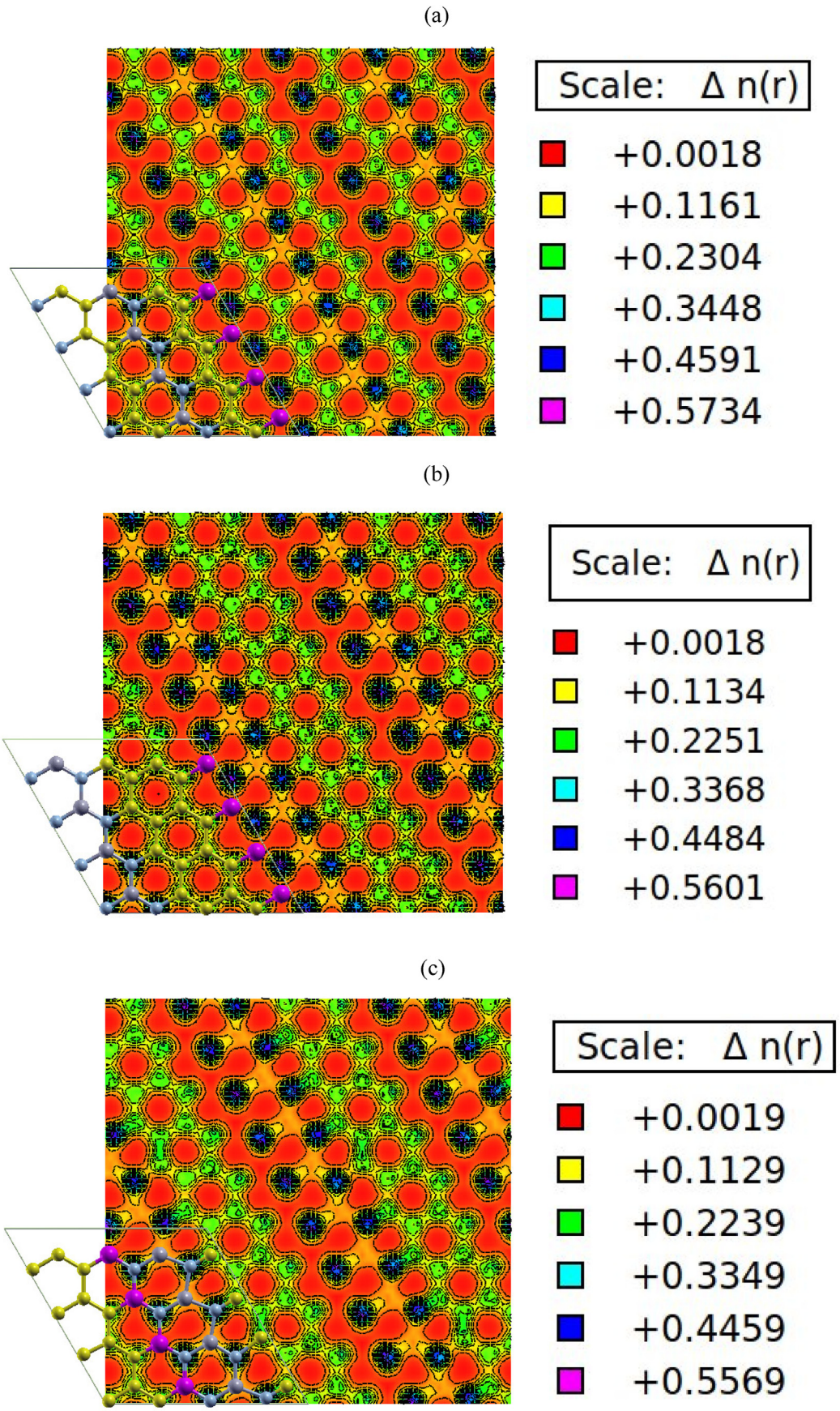

Fig. 7. Calculated self-consistent charge density isolines and isosurfaces of (a) AlN:CC:BN, (b) AlN:CC:CC:BN and (c) CC:BN:AlN:CC nanoheterostructure configurations. The rainbow type color-coding refers to violet as regions of maximum charge density which decreases gradually finally to red as region of minimum charge density. (For interpretation of the references to color in this figure legend, the reader is referred to the Web version of this article.)

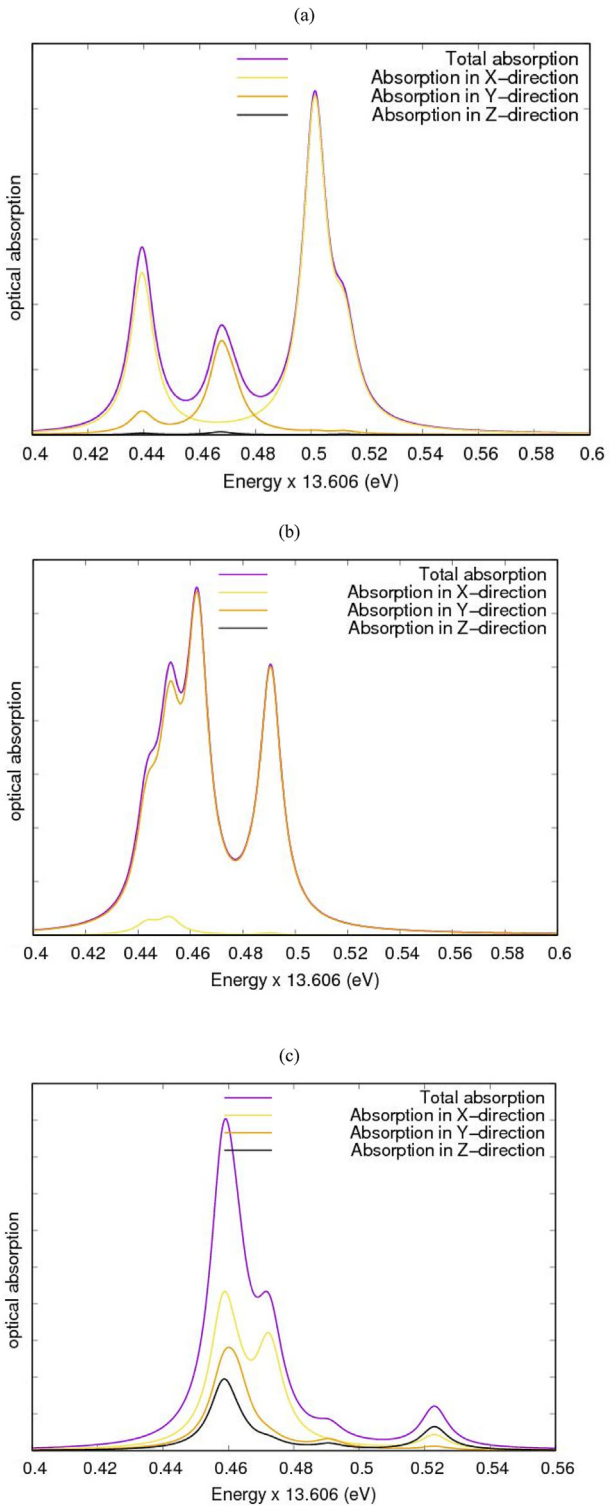

Fig. 8. Calculated optical absorption spectra of (a) AlN:CC:BN, (b) AlN:CC:CC:BN and (c) CC:BN:AlN:CC nanoheterostructure configurations.

optoelectronic technology due to their orientation dependent and frequency dependent properties. These low symmetrical systems with diverse properties and features can become solution for frequency and direction dependent devices due to their anisotropy.

4. Conclusions

The current manuscript described the application of DFT in designing novel nanoheterostructures. We investigated the ground-state structural, electronic and optical properties of novel 2D nanoheterostructures from 2D graphene, aluminium nitride and boron nitride. We discussed the stability through calculation of formation energies of different nanoheterostructures, investigating three different doping patterns for CC:AlN:BN nanoheterostructures. The calculated band gaps of the novel nanoheterostructures are found to be 0.87, 0.43 and 0.65 eV respectively. These novel hybrid 2D nanoheterostructures are found to exhibit both direct and indirect band gaps. They have tunable band gaps and have potential applications in nanoscale semiconducting and optoelectronic devices, notably optical, optoelectronic and micro-electro-mechanical systems. With these proposed bandgap tuning nanoheterostructures, one may expect the property-oriented designs of B, C, N, Al-based nanoheterostructures to meet the ever-growing demands of future high-performance devices in optical, optoelectrical, imaging, sensing and other electronic application fields. These results may provide guidance in practical engineering applications, specifically to tune the band gap in 2D materials. Finally, our results are useful to provide an explanation of the formation of hybridized 2D nanomaterials. This new form of hybridized 2D material facilitates the development of band gap engineering and applications, in particular, in nanoelectronics and nano-optics. To generalize, we would like to emphasize that DFT calculations should not only be considered useful for studying some selected cases, i.e., compounds with a given composition as in the present case, but they are very useful to produce a database for searching a large space of possible structural configurations. Our case study could provide some guidelines for the industrialists and academic scientists in the development of new materials.

Funding

This research received no external funding.

Conflict of interest disclosure

The author(s) declare(s) that there is no conflict of interest regarding the publication of this paper.

Data availability statement

The DFT data used to support the findings of this study are included within the article.

Declaration of competing interest

The authors declare that they have no known competing financial interests or personal relationships that could have appeared to influence the work reported in this paper.

Acknowledgments

The authors would like to acknowledge the financial support from the Ghana Government Book and Research Allowance for tertiary institutions. V. W. E., acknowledges financial support from the University of Ghana Pan African Doctoral Academy. Authors are grateful to the Centre for High Performance Computing (CHPC), Cape Town, South Africa, for computer time on the Lengau" cluster.

References

[1] R.S. Pease, An X-ray study of boron nitride, Acta Crystallogr. 5 (1952) 356–361.
[2] F.P. Bundy, R.H. W Jr., Direct transformation of hexagonal boron nitride to denser forms, J. Chem. Phys. 38 (1963) 1144–1149.
[3] T. Soma, A. Sawaoka, S. Saito, Characterization of wurtzite type boron nitride synthesized by shock compression, Mater. Res. Bull. 9 (1974) 755–762.
[4] F.R. Corrigan, F.P. Bundy, Direct transitions among the allotropic forms of boron nitride at high pressures and temperatures, J. Chem. Phys. 63 (1975) 3812–3820.

[5] R.H. W Jr., Cubic form of boron nitride, 956-956, J. Chem. Phys. 26 (1957).
[6] K. Eichhorn, A. Kirfel, J. Grochowski, P. Serda, Accurate structure analysis with synchrotron radiation. An application to borazone, cubic BN, Acta Crystallogr. B 47 (1991) 843–848.
[7] K. Doll, J.C. Schon, M. Jansen, Structure prediction based on ab initio simulated ϵ annealing for boron nitride, Phys. Rev. B 78 (2008), 144110.
[8] L. Vel, G. Demazeau, J. Etourneau, Cubic boron nitride: synthesis, physicochemical properties and applications, Mater. Sci. Eng., B 10 (1991) 149–164.
[9] L.M. Gameza, V.B. Shipilo, V.A. Savchuk, Kinetic features of crystallization of cubic boron nitride single crystals in the BN-LiH(N,Se) system, Phys. Status Solidi 198 (1996) 559–563.
[10] Y. Matsui, Small particles of cubic boron nitride prepared by electron irradiation of hexagonal boron nitride in a transmission electron microscope, J. Cryst. Growth 66 (1984) 243–247.
[11] H. Wang, H. Xu, X. Wang, C. Jiang, High-pressure lattice dynamics and thermodynamic properties of zinc-blende BN from first-principles calculation, Phys. Lett. 373 (2009) 2082–2086.
[12] T. Takayama, M. Yuri, K. Itoh, T. Baba, J.S. Harris Jr., Analysis of phase-separation region in wurtzite group III nitride quaternary material system using modified valence force field model, J. Cryst. Growth 222 (2001) 29–37.
[13] X. Wei, M.-S. Wang, Y. Bando, D. Golberg, Electron-beam-induced substitutional carbon doping of boron nitride nanosheets, nanoribbons, and nanotubes, ACS Nano 5 (2011) 2916–2922.
[14] L. Ci, L. Song, C. Jin, D. Jariwala, D. Wu, Y. Li, A. Srivastava, Z.F. Wang, K. Storr, L. Balicas, F. Liu, P.M. Ajayan, Atomic layers of hybridized boron nitride and graphene domains, Nat. Mater. 9 (2010) 430–435.
[15] S. Tang, Z. Cao, Carbon-doped zigzag boron nitride nanoribbons with widely tunable electronic and magnetic properties: insight from density functional calculations, Phys. Chem. Chem. Phys. 12 (2010) 2313–2320.
[16] Y.J. Cho, C.H. Kim, H.S. Kim, J. Park, H.C. Choi, H.-J. Shin, G. Gao, H.S. Kang, Electronic structure of Si-doped BN nanotubes using X-ray photoelectron spectroscopy and first-principles calculation, Chem. Mater. 21 (2009) 136–143.
[17] Y.-j. Liu, B. Gao, D. Xu, H.-m. Wang, J.-x. Zhao, Theoretical study on Si-doped hexagonal boron nitride (h-BN) sheet: electronic, magnetic properties, and reactivity, Phys. Lett. 378 (2014) 2989–2994.
[18] Q.u.A. Asif, A. Hussain, A. Nabi, M. Tayyab, H.M. Rafique, Computational study of X-doped hexagonal boron nitride (h-BN): structural and electronic properties (X = P, S, O, F, Cl), J. Mol. Model. 27 (2021) 31.
[19] Z.C. Feng, III-Nitride Semiconductor Materials, Imperial College Press, London, 2006.
[20] B. Ul Haq, S. AlFaify, R. Ahmed, F.K. Butt, K. Alam, Z. Tariq, S. Ur Rehman, Structural, electronic, and optical properties of the pressure-driven novel polymorphs of gallium nitride: first-principles investigations, Int. J. Energy Res. 46 (2022) 2361–2372.
[21] S. Daoud, N. Bouarissa, Structural and thermodynamic properties of cubic sphalerite aluminum nitride under hydrostatic compression, Computat. Condensed Matter. 19 (2019), e00359.
[22] B. Pecz, G. Nicotra, F. Giannazzo, R. Yakimova, A. Koos, A. KakanakovaGeorgieva, Indium nitride at the 2D limit, Adv. Mater. 33 (2021), 2006660.
[23] H. Heidari, S. Afshari, E. Habibi, Sensing properties of pristine, Al-doped, and defected boron nitride nanosheet toward mercaptans: a first-principles study, RSC Adv. 5 (2015) 94201–94209.
[24] S. Muniyandi, R. Sundaram, T. Kar, Aluminum doping makes boron nitride nanotubes (BNNTs) an attractive adsorbent of hydrazine (N2H4), Struct. Chem. 29 (2018) 375–382.
[25] Z. Liu, S. Zhao, T. Yang, J. Zhou, Improvement in mechanical properties in AlN-h-BN composites with high thermal conductivity, J. Adv. Ceramics 10 (2021) 1317–1325.
[26] Q. Zhang, Q. Li, W. Zhang, H. Zhang, F. Zheng, M. Zhang, P. Hu, M. Wang, Z. Tian, Y. Li, Y. Liu, F. Yun, Phase transition and bandgap engineering in B1-xAlxN alloys: DFT calculations and experiments, Appl. Surf. Sci. 575 (2022), 151641.
[27] H. Ahmoum, M. Boughrara, M. Kerouad, Electronic and magnetic properties of Al doped (w-BN) with intrinsic vacancy, Superlattice, Microst 127 (2019) 186–190.
[28] M. Mirzaei, A. Nouri, The Al-doped BN nanotubes: a DFT study, J. Mol. Struct.: THEOCHEM 942 (2010) 83–87.
[29] A.A. Peyghan, M. Noei, S. Yourdkhani, Al-doped graphene-like BN nanosheet as a sensor for para-nitrophenol: DFT study, Superlattice, Microst 59 (2013) 115–122.
[30] S. Yu, L. Li, Z. Lai, J. Hao, K. Zhang, A coupling effects of vacancy and Al (Ga, In) dopant on electronic structures of hexagonal boron nitride monolayer, Mater. Res. Express 4 (2017), 116302.
[31] D.M.S. Shanmugan, Performance of chemical vapor deposited boron-doped AlN thin film as thermal interface materials for 3-W LED: thermal and optical analysis, Acta Metall. Sin. 31 (2018) 97–104.
[32] S. Subramani, M. Devarajan, Testing and Analysis of Boron-Doped Aluminum Nitride Thin-Film-Coated Al as Thermal Substrates in PCB Fabrication for LED Application, vol. 63, 2016, pp. 4839–4844.
[33] M. Zhang, X. Li, Structural and electronic properties of wurtzite BxAl1–xN from first-principles calculations, Phys. Status Solidi 254 (2017), 1600749.
[34] V. Ilyasov, T. Zhdanova, I. Nikiforov, Structural and electronic properties of AlN and BN wide-gap semiconductors and their BxAl1-xN solid solutions, J. Struct. Chem. 46 (2005) 791–798.
[35] E. Viswanathan, M. Sundareswari, S. Krishnaveni, M. Manjula, D.S. Jayalakshmi, Theoretical investigation on effect of boron on improving the hardness of zincblende-aluminium nitride and its mechanical, thermal and thermoelectric properties, J. Superhard Mater. 41 (2019) 321–333.
[36] L.K. Teles, J. Furthmüller, L.M.R. Scolfaro, A. Tabata, J.R. Leite, F. Bechstedt, T. Frey, D.J. As, K. Lischka, Phase separation and gap bowing in zinc-blende InGaN, InAlN, BGaN, and BAlN alloy layers, Phys. E Low-dimens. Syst. Nanostruct. 13 (2002) 1086–1089.
[37] S. Kumar, S. Joshi, B. Joshi, S. Auluck, Thermodynamical and electronic properties of BxAl1-xN alloys: a first principles study, J. Phys. Chem. Solid. 86 (2015) 101–107.
[38] M. Mbarki, R. Alaya, A. Rebey, Ab initio investigation of structural and electronic properties of zinc blende AlN1-xBix alloys, Solid State Commun. 155 (2013) 12–15.
[39] R. Riane, Z. Boussahla, S.F. Matar, A. Zaoui, Structural and electronic properties of zinc blende-type nitrides BxAl1–xN, Z. Naturforsch. B Chem. Sci. 63 (2008) 1069–1076.
[40] B. Ghebouli, M.A. Ghebouli, M. Fatmi, Theoretical studies of structural, elastic, electronic and lattice dynamic properties of AlxYyB1-x-yN quaternary alloys, Phys. B Condens. Matter 406 (2011) 2521–2527.
[41] R. Yang, C. Zhu, Q. Wei, Z. Du, First-principles study of the properties of Pmn21-B1–xAlxN, Phil. Mag. 97 (2017) 3008–3026.
[42] G.C. Jimenez, Cesar O. Lopez, M.J. Espitia R, Theoretical investigation of the electronic and magnetic properties of TM (TM¼Ti, V, and Cr)-doped w-BN compound, J. Magn. Magn Mater. 402 (2016) 156–160.
[43] M.J. Espitia R, J.H. Díaz F, J.A. Rodríguez Martínez, Structural and electronic properties of V-doped cubic BN: a density functional theory study, Solid State Commun. 244 (2016) 23–27.
[44] M. Mirzaei, A. Nouri, The Al-doped BN nanotubes. ADFT study, J Mol Struct, THEOCHEM. 942 (2010) 1 83–87.
[45] A.A. Peyghan, M. Noei, S. Yourdkhani, Al-doped graphene-like BN nanosheet as a sensor for para-nitrophenol. DFT study, Superlattice. Microst. 59 (2013) 115–122.
[46] S. Yu, L. Li, Z. Lai, J. Hao, K. Zhang, A coupling effects of vacancy and Al (Ga, In) dopant on electronic structures of hexagonal boron nitride monolayer, Mater. Res. Express 4 (11) (2017), 116302.
[47] J. Zagorac, D. Zagorac, B. Babić, T. Prikhna, B. Matović, Effect of aluminum addition on the structure and electronic properties of boron nitride, J. Solid State Chem. 311 (2022), 123153.
[48] D. Zagorac, J. Zagorac, M. Fonović, T. Prikhna, B. Matović, Novel boron-rich aluminum nitride advanced ceramic materials, Int. J. Appl. Ceram. Technol. 20 (2023) 174–189, https://doi.org/10.1111/ijac.14152.
[49] H. Ahmoum, M. Boughrara, M. Kerouad, Electronic and magnetic properties of Al doped (w−BN) with intrinsic vacancy, Superlattice. Microst. 127 (2019) 186–190.
[50] B.G. Streetman, S. Banerjee, in: Solid State Electronic Devices, seventh ed., Prentice-Hall, Englewood Cliffs, NJ, 1995.
[51] J. Wilson, J.F. Hawkes, in: Optoelectronics – an Introduction, second ed., Prentice Hall, Englewood Cliffs, NJ, 1989.
[52] A.K. Geim, K.S. Novoselov, Nat. Mater. 6 (2007) 183–191.
[53] K.S. Novoselov, et al., Science 306 (2004) 666–669.
[54] A.K. Geim, Science 324 (2009) 1530–1534.
[55] A.H. Castro Neto, F. Guinea, N.M.R. Peres, K.S. Novoselov, A.K. Geim, Rev. Mod. Phys. 81 (2009) 109–162.
[56] A. Splendiani, et al., Nano Lett. 10 (2010) 1271–1275.
[57] K.S. Novoselov, et al., Proc. Natl. Acad. Sci. USA 102 (2005) 10451–10453.
[58] Van W. Elloh, Yaya Abu, G. Gebreyesus, Piyush Dua, Abhishek K. Mishra, New 2D structural materials: carbon−Gallium nitride (CC−GaN) and Boron−Gallium nitride (BN−GaN) heterostructures – materials design through density functional theory, ACS Omega 4 (2019) 1722–1728, https://doi.org/10.1021/acsomega.8b03025.
[59] B. Radisavljevic, A. Radenovic, J. Brivio, V. Giacometti, A. Kis, Nat. Nanotechnol. 6 (2011) 147–150.
[60] H. Wang, et al., Nano Lett. 81 (2012) 109–162.
[61] R.S. Sundaram, et al., Nano Lett. 13 (2013) 1416–1421.
[62] M. Bernardi, C. Ataca, M. Palummo, J.C. Grossman, Optical and electronic properties of two-dimensional layered materials, Nanophotonics 6 (2017) 479–493, https://doi.org/10.1515/nanoph-2015-0030.
[63] B. Mortazavi, F. Shojaei, M. Azizi, T. Rabczuk, X. Zhuang, As2S3, As2Se3 and As2Te3 nanosheets: superstretchable semiconductors with anisotropic carrier mobilities and optical properties, J. Mater. Chem. C 8 (2020) 2400–2410, https://doi.org/10.1039/C9TC05904K.
[64] S. Zhang, S. Guo, Z. Chen, Y. Wang, H. Gao, J. Gómez-Herrero, P. Ares, F. Zamora, Z. Zhu, H. Zeng, Recent progress in 2D group-VA semiconductors: from theory to experiment, Chem. Soc. Rev. 47 (2018) 982–1021, https://doi.org/10.1039/C7CS00125H.
[65] M. Šiškins, M. Lee, F. Alijani, M.R. Van Blankenstein, D. Davidovikj, H.S.J. Van Der Zant, P.G. Steeneken, Highly anisotropic mechanical and optical properties of 2D layered As_2S_3 membranes, ACS Nano 13 (2019) 10845–10851, https://doi.org/10.1021/acsnano.9b06161.
[66] A. Patel, D. Singh, Y. Sonvane, P.B. Thakor, R. Ahuja, Bulk and monolayer As2S3 as promising thermoelectric material with high conversion performance, Comput. Mater. Sci. 183 (2020), 109913, https://doi.org/10.1016/j.commatsci.2020.109913.
[67] A. Gupta, T. Sakthivel, S. Seal, Prog. Mater. Sci. 73 (2015) 44.
[68] Q.H. Wang, K. Kalantar-Zadeh, A. Kis, J.N. Coleman, M.S. Strano, Nat. Nanotechnol. 7 (2012) 699.
[69] F. Xia, H. Wang, D. Xiao, M. Dubey, A. Ramasubramaniam, Nat. Photonics 8 (2014) 899.
[70] F. Yang, S. Cheng, X. Zhang, X. Ren, R. Li, H. Dong, W. Hu, Adv. Mater. 30 (2018), 1702415.
[71] M. Xu, T. Liang, M. Shi, H. Chen, Chem. Rev. 113 (2013) 3766.

[72] P. Giannozzi, S. Baroni, N. Bonini, et al., Quantum espresso: a modular and open-source software project for quantum simulations of materials, J. Phys. 21 (39) (2009). Article ID 395502.
[73] D. Vanderbilt, Soft self-consistent pseudopotentials in a generalized eigenvalue formalism. The Pseudopotential generation, Phys. Rev. B 41 (1990) 7892.
[74] H.J. Monkhorst, J.D. Pack, Special points for Brillouin-zone integrations, Phys. Rev. B 13 (1976) 5188–5192.
[75] S. Grimme, J. Antony, S. Ehrlich, H. Krieg, A consistent and accurate ab initio parametrization of density functional dispersion correction (DFT-D) for the 94 elements H-Pu, J. Chem. Phys. 132 (2010), 154104.